

SeasonDepth: Cross-Season Monocular Depth Prediction Dataset and Benchmark under Multiple Environments

Hanjiang Hu, Baoquan Yang, Weiang Shi, Zhijian Qiao, and Hesheng Wang*

Abstract—Monocular depth prediction has been well studied recently, while there are few works focused on the depth prediction across multiple environments, *e.g.* changing illumination and seasons, owing to the lack of such real-world dataset and benchmark. In this work, we derive a new cross-season scaleless monocular depth prediction dataset *SeasonDepth*¹ from *CMU Visual Localization* dataset through structure from motion. And then we formulate several metrics to benchmark the performance under different environments using recent state-of-the-art open-source depth prediction pretrained models from *KITTI* benchmark. Through extensive zero-shot experimental evaluation on the proposed dataset, we show that the long-term monocular depth prediction is far from solved and provide promising solutions in the future work, including geometric-based or scale-invariant training. Moreover, multi-environment synthetic dataset and cross-dataset validation are beneficial to the robustness to real-world environmental variance.

I. INTRODUCTION

Outdoor monocular depth prediction plays an essential role in the perception of autonomous driving and mobile robotics. In recent years, monocular depth prediction has made significant progress due to the boost of deep convolutional neural networks [1]–[4]. However, since the outdoor environmental condition is changing due to different seasons, weather and day time [5], the pixel appearance is drastically affected, which poses a huge challenge for the robust visual perception and localization.

For the consideration of the cross-dataset performance [6], especially under adverse environment for depth prediction [7], it is of great necessity to study how environmental changes influence the monocular depth prediction. Besides, cross-season real-world datasets and benchmark would also promote the related tasks [8], like long-term visual localization [9] and place recognition [10].

Since the groundtruth of the outdoor depth map is usually sparse from the calibrated LiDAR device, and it is expensive and effort-costly to obtain high-quality dense depth map, we derive a scaleless dense depth prediction dataset *SeasonDepth* with multi-environment traverses based on the urban part of *CMU Localization* dataset [11]. Different from dataset

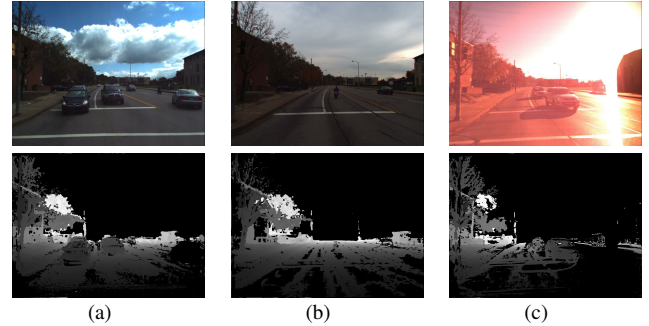


Fig. 1. The first row shows the image samples in the proposed dataset *SeasonDepth* and the second row gives the ground truths. Column (a) is under *Cloudy + Foliage* condition, (b) is under *Overcast + Mixed Foliage* condition and (c) is under *Low Sun + Mixed Foliage* condition.

with dense depth map from stereo camera, we adopt structure from motion (SfM) and multi-view stereo (MVS) pipeline with clustering-based RANSAC to filter the dynamic objects on the road, followed by the refinement in HSV color space for the areas with extreme illumination change.

To benchmark the performance on the dataset, several practical metrics are proposed for the zero-shot evaluation of the state-of-the-art open-source methods with pretrained models from *KITTI* benchmark [12], [13] on *SeasonDepth*. The baselines we choose include supervised [14]–[16], semi-supervised [17] and self-supervised [18]–[21] algorithms trained on the real-world dataset and domain adaptation algorithms [22], [23] trained on the virtual synthetic dataset with changing environments [24]. From the evaluation results, no robust algorithm could solve the problem of depth prediction under changing environments. And promising avenues in geometric constraint, normal-based and scale-invariant training are found. Furthermore, it is shown that cross-dataset validation and model training on multi-environment virtual dataset are also helpful to the robustness to the real-world changing environments. In summary, our contributions in this work lie in:

- A new monocular depth prediction dataset *SeasonDepth* with drastic environmental changes is built and available through MVS pipeline with modified RANSAC for refinement.
- Several metrics are proposed to measure the depth map with relative depth value under multiple environments, evaluating the effectiveness and robustness for each algorithm.
- Recent state-of-the-art open-sourced depth prediction algorithms are evaluated on the *SeasonDepth* with pretrained model on *KITTI* benchmark, showing what kind of methods are robust to changing environments.

This work was supported in part by the Natural Science Foundation of China under Grant U1613218, 61722309 and U1913204, in part by Beijing Advanced Innovation Center for Intelligent Robots and Systems under Grant 2019IRS01. Corresponding Author: Hesheng Wang.

The authors are with Department of Automation, Institute of Medical Robotics, Key Laboratory of System Control and Information Processing of Ministry of Education, Key Laboratory of Marine Intelligent Equipment and System of Ministry of Education, Shanghai Jiao Tong University, Shanghai 200240, China. H. Wang is also with Beijing Advanced Innovation Center for Intelligent Robots and Systems, Beijing Institute of Technology, China

¹Available on <https://github.com/SeasonDepth/SeasonDepth>.

The rest of the paper is structured as follows. Section II analyzes the related work in monocular depth prediction and related datasets. Section III presents the proposed dataset. Section III introduces the metrics and benchmark setup. The experimental evaluation is shown in Section IV. Finally, in Section VI we draw the conclusions.

II. RELATED WORK

A. Depth Prediction Datasets

Depth prediction plays an important role in the application of perception and localization of mobile robotics and other computer vision applications. The dataset is essential to the development of depth prediction task. The acquirement of the depth map ground truth is challenging for the dataset, and it would be obtained through other calibrated devices or complicated calculating algorithms. For the indoor scenarios, the ground truth of depth map is quite easy to get directly through the calibrated RGBD camera like [25]–[27], web stereo photos like [16], [28], [29] or sparse depth map from laser scanner like [30].

While the ground truth of outdoor depth map is more complex to obtain, one common method is to project the LiDAR point cloud data onto the image plane [12], [21], [30], which is quite accurate but too sparse and thus needs inaccurate interpolation for dense depth map. And the stereo camera includes two aligned cameras which generate the disparity map through stereo matching and depth calculating algorithms, like *CityScapes* dataset [31]. But the calculation has theoretical drawbacks of the limited depth scope which is determined by the baseline of the stereo camera. And the stereo matching is sensitive to the illumination variance of image pairs as well. Another way to get the depth map is through image geometric registration [15], [32], which helps to recover the 3D dense model by feature matching from monocular sequence. Although this method is time-consuming, it generates pretty accurate dense depth maps with relative scale, which is more general for depth prediction under different scenarios. *Megadepth* [15] is the most similar one to our proposed dataset, where structure from motion method is implemented to reconstruct the 3D model and depth map. However, the images are from the Internet so they are not multi-traverse with different environments with lots of dynamic objects.

Changing environments casts great challenge on the outdoor visual perception and localization of mobile robots, which gives significant necessity to build a new dataset with multiple environments. Though [31] includes some environmental changes, there are still no real-world dataset with multi-environment traverses, which is really important to the evaluation of the generalization ability across environmental changes and could be found in some virtual synthetic datasets [24], [33]. The synthetic depth maps are of high quality while the RGB images are obviously different from real-world images, and therefore domain adaptation is indispensable when training on it. The details of comparison of datasets are shown in Section III-C.

B. Outdoor Monocular Depth Prediction Algorithms

Since the depth map cannot be directly obtained through monocular camera in the outdoor scenarios, monocular depth prediction aims to predict the depth map given single RGB image. Early studies including MRF and other graph models [30], [34], [35] largely depend on man-made descriptors so as to constrain the performance of depth prediction. Afterwards, enormous studies on convolutional neural networks [1]–[3], [36] have shown promising results for monocular depth estimation. Among these, [2] combines neural networks with continuous CRF pixel by pixel, which is different from the regression task for depth prediction. Recent work [37] analyzes the mechanism of inferring depth maps from monocular images through CNNs. Supervised methods [15], [16] and semi-supervised methods [17] for monocular depth prediction have been well studied through the supervision of depth map ground truth. Recently, normal-based methods [14], [38], [39] have been proposed to regress the normal and depth map using the geometric constraints.

However, since the groundtruth of outdoor depth map is effort-costly and time-consuming to obtain, some unsupervised learning methods [18], [40]–[44] for depth estimation have appeared to solve this problem using stereo geometry information as a secondary supervisory signal. Furthermore, in [43], depth prediction has even been coped with as image reconstruction in an unsupervised manner. Additionally, left-right consistency [20], [40] and ego-motion pose constraint [44] have also been exploited in self-supervised [19], [21], [41], [45] way to estimate depth map.

Also, to avoid using the expensive real-world depth map ground truth, other algorithms are trained on the multi-environment synthetic virtual datasets [24] to leverage the high-quality depth map. Such methods [22], [23], [46], [47] confront with the domain adaptation from synthetic domain to real-world domain through training the model on the virtual datasets.

III. SEASONDEPTH DATASET

To study how depth prediction performance are influenced by environmental factors, a new dataset *SeasonDepth* is derived from CMU Visual Localization dataset [11] through SfM method with clustering-based RANSAC and HSV filtering refinement. The original CMU Visual Localization dataset [11] covers over 12 months in Pittsburgh, USA, including 12 different environmental conditions. It was collected from two cameras on the left and right of the vehicle along 8.5 kilometers. And this dataset is also used for long-term visual localization [5] by calculating the 6-DoF camera pose of images under different environments. We adopt Urban area according to the categorization in [5] with 7 slices about 21652 images in total for the city-view scenarios in mobile robotics and autonomous driving. The different conditions consist of multiple weather and season conditions with the combination of sunny, cloudy, overcast, low sun and snow together with foliage, mixed foliage and no foliage. Some examples of the dataset are shown in Figure 2.

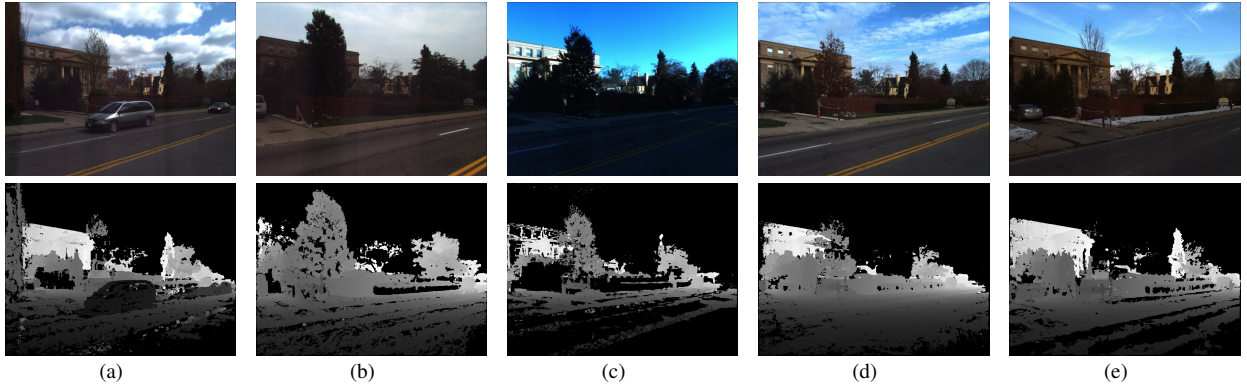


Fig. 2. Column (a) (b) (c) (d) (e) present the examples and depth map groundtruths of *SeasonDepth* dataset, which are under *Sunny + No Foliage*, *Overcast + Foliage*, *Low Sun + Mixed Foliage*, *Cloudy + Mixed Foliage* and *Cloudy + Foliage* condition respectively.

A. Image Reconstruction with Clustering-based RANSAC

We reconstruct the dense model for each traversal under every environmental condition through multi-view stereo (MVS) pipeline [48]. Specifically, COLMAP [48], [49] is used to obtain the depth maps through photometric and geometric consistency from sequential images. To make full use of the image sequences, we adjust the sequential matching overlap to be 15 instead of the whole sequence, improving the local optimization with less noise.

Since there are many dynamic objects along the road for every image sequence, we devise a modified RANSAC algorithm along with MVS pipeline based on COLMAP. During each iteration of RANSAC algorithm in triangulation, first all the depth of the pixels are reconstructed even with lots of noise due to dynamic objects, and then K-means clustering is implemented based on the 3D distance. After roughly clustering, the inliers would be found and the outliers would be calculated based on the maximum relative matching distance of 0.55. The whole cluster with the inlier ratio of less than 50% will be labeled as outliers as well. After optimizing the camera pose and depth value of inliers through bundle adjustment, the iteration continues until the total inlier ratio surpasses the minimum inlier ratio of 0.65 and the outliers will be set to be empty value finally. The example of filtering dynamic object could be found in Figure 3-(a).

Also, the MVS algorithm generates the ground truth maps with some error points which are greatly out of range or too close, like the cloud in the sky or noisy points on the very near road. Consequently, the points which exceed the normal range of the depth map are rejected. Pixels between 5 % and 92% of the largest original depth are kept, which maintains the valid pixels of the original depth map as much as possible and rejects most noise pixels.

B. Depth Map Refinement

Although refinement based on semantic segmentation is commonly used in previous work [15] after SfM, it is really challenging to generate the semantic segmentation map for the images under drastically changing environments for the dataset. Instead, we adopt simple but effective noise filtering method for refinement. After the depth maps are generated

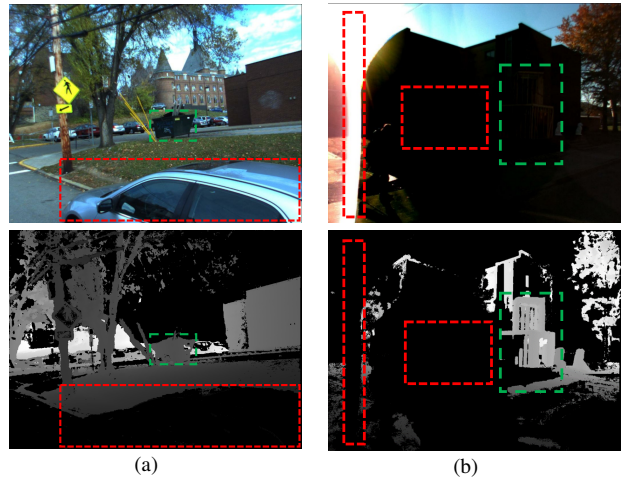


Fig. 3. The filtered areas are shown in dashed red blocks while the reconstructed areas are shown in dashed green blocks. Column (a) shows the effect of RANSAC to remove the dynamic object while keeping the static objects. Column (b) shows the effective refinement in the HSV color space for special noisy areas.

from COLMAP, we have investigated the noise distribution with respect to the pixel value in the color space, like blue pixels always appear in the sky which tends to be noise in most cases. Instead of filtering the noise pixels in the RGB color space, we use the HSV color space to remove the noisy area. For most clear or cloudy sky, the Value tends to be high about 100 and the Hue is usually blue or white. However, for those area in the shadow of low sun, the Saturation and Value are extremely low to be around 10 so that the depth map pixels are too hard to be correctly reconstructed, which need to be filtered. The sample of filtering in HSV space is shown in Figure 3-(b). Since the pixels of the near road rarely overlap from the multiple views for local optimization, noise of these areas often occurs and is far beyond the range of its neighboring pixels. These noise pixels of depth map could be filtered through the specific position on the image.

C. Comparison with Other Datasets

The current datasets are introduced in II-A. The comparison between *SeasonDepth* and several popular datasets is shown in Table I. *SeasonDepth* contains comprehensive and multiple outdoor real-world environmental conditions for

TABLE I
COMPARISON BETWEEN *SeasonDepth* AND OTHER DATASETS

Name	Scene	Real or Virtual	Depth Value	Sparse or Dense	Multiple Traverses	Different Environments	Dynamic Objects
NYUV2 [25]	Indoor	Real	Absolute	Dense	×	×	✓
DIML [26]	Indoor	Real	Absolute	Dense	×	×	×
iBims-1 [27]	Indoor	Real	Absolute	Dense	×	×	×
Make3D [30]	Outdoor & Indoor	Real	Absolute	Sparse	×	×	×
ReDWeb [29]	Outdoor & Indoor	Real	Relative	Dense	×	×	✓
WSVD [28]	Outdoor & Indoor	Real	Relative	Dense	×	×	✓
HR-WSI [16]	Outdoor & Indoor	Real	Absolute	Dense	×	×	✓
KITTI [12]	Outdoor	Real	Absolute	Sparse	×	×	✓
CityScapes [31]	Outdoor	Real	Absolute	Dense	×	✓	✓
DIW [32]	Outdoor	Real	Relative	Sparse	×	×	✓
MegaDepth [15]	Outdoor	Real	Relative	Dense	×	×	✓
DDAD [21]	Outdoor	Real	Absolute	Dense	×	×	✓
V-KITTI [24]	Outdoor	Virtual	Absolute	Dense	✓	✓	✓
SYNTHIA [33]	Outdoor	Virtual	Absolute	Dense	×	×	×
SeasonDepth	Outdoor	Real	Relative	Dense	✓	✓	×

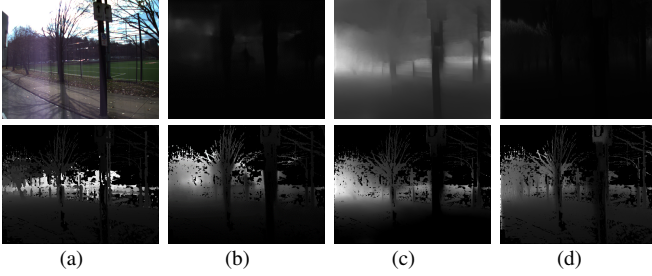


Fig. 4. The example of depth adjustment and normalization of evaluation result. Column (a) shows the RGB image and depth map groundtruth. Column (b) (c) (d) are results of *PackNet* [21], *VNL* [14] and *GASDA* [23]. The depth maps on the first row are the original depth output while those on the second row are the adjusted depth map results through Equation (1).

every scene sequence as the synthetic virtual dataset *V-KITTI* does. Though *CityScapes* includes different environments, it lacks the traverses under different conditions so is not able to evaluate the performance across changing environments. Similar to outdoor *DIW* and *MegaDepth* dataset, the depth map of ours is scaleless and it contains the relative depth value and geometry of the images, where the values need to be normalized for evaluation as the following section shows. The depth map ground truths are dense compared to LiDAR-based sparse depth maps. Also, dynamic objects are removed to be empty through RANSAC but static vehicles are kept, which ensures the diversity of objects for evaluation.

IV. BENCHMARK SETUP

In this section, several metrics are proposed for *SeasonDepth* to benchmark state-of-the-art open-source algorithms with pretrained models on *KITTI* benchmark [13].

A. Evaluation Metrics

The challenge for the evaluation lies in two points, and one is to cope with the scaleless and partially-valid dense depth map ground truth. While the other is to find appropriate metrics to fully measure the depth prediction performance across different environments.

In the *SeasonDepth* dataset, the scale of the ground truth depth map ground truth generated from SfM method is relative. In order to adapt to other algorithms which predict depth maps with absolute scale, different from the way [44]

does, the predicted depth maps from all of these depth estimation methods are normalized to meet the scaleless ground truth based on both the mean value and variance with the assumption of Gaussian distribution, aligning the distribution of predicted map to groundtruth. First, for each predicted and groundtruth map, the valid pixels $D_{valid_predicted}^{i,j}$ of the predicted depth map $D_{valid_predicted}$ are determined by the correspondence with the non-empty or valid pixels $D_{valid_GT}^{i,j}$ of the depth map ground truth. And then the valid average and variance value of both D_{valid_GT} and $D_{valid_predicted}$ are calculated as Avg_{GT} , Avg_{pred} and Var_{GT} , Var_{pred} . Then we use this formula to normalize the depth map D_{adj} to have the same distribution with D_{valid_GT} ,

$$D_{adj} = (D_{pred} - Avg_{pred}) \times \sqrt{\frac{Var_{GT}}{Var_{pred}}} + Avg_{GT} \quad (1)$$

After this operation, we could reduce the difference of scales for the current methods across datasets, which makes this zero-shot evaluation dataset reliable and usable in all models no matter what datasets they were trained on, improving the robustness and accuracy for the evaluation for generalization ability. Denote the adjusted valid predicted depth map D_{adj} in Equation (1) as D_P in the following formulation. The results of adjusted depth prediction are shown in Figure 4.

The most commonly used evaluation metrics for monocular depth prediction are *AbsRel*, *SqRel*, *RMSE*, *RMSElog*, *SILog*, $\delta < 1.25$, $\delta < 1.25^2$ and $\delta < 1.25^3$ [13]. However, for the evaluation under changing environments, we choose the most distinguishable metrics under multiple environments, *AbsRel* and $\delta < 1.25$ (a_1), to benchmark the performance of baselines. For environment k , *AbsRel* ^{k} and a_1^k are calculated in Equation (2) and (3).

$$AbsRel^k = \frac{1}{n} \sum_{i,j}^n |D_P^k{}_{i,j} - D_{GT}^k{}_{i,j}| / D_{GT}^k{}_{i,j} \quad (2)$$

$$a_1^k = \frac{1}{n} \sum_{i,j}^n \mathbb{1}(\max\{\frac{D_P^k{}_{i,j}}{D_{GT}^k{}_{i,j}}, \frac{D_{GT}^k{}_{i,j}}{D_P^k{}_{i,j}}\} < 1.25) \quad (3)$$

For the evaluation under different environments, six secondary metrics are proposed based on these original metrics

in the Equation (4)-(9).

$$AbsRel^{avg} = \frac{1}{m} \sum_k AbsRel^k \quad (4)$$

$$AbsRel^{var} = \frac{1}{m} \sum_k \left| AbsRel^k - \frac{1}{m} \sum_k AbsRel^k \right|^2 \quad (5)$$

$$AbsRel^{dev} = \frac{(\max\{AbsRel^k\} - \min\{AbsRel^k\})}{\frac{1}{m} \sum_k AbsRel^k} \quad (6)$$

$$a_1^{avg} = \frac{1}{m} \sum_k a_1^k \quad (7)$$

$$a_1^{var} = \frac{1}{m} \sum_k \left| a_1^k - \frac{1}{m} \sum_k a_1^k \right|^2 \quad (8)$$

$$a_1^{dev} = \frac{(\max\{1 - a_1^k\} - \min\{1 - a_1^k\})}{\frac{1}{m} \sum_k (1 - a_1^k)} \quad (9)$$

where *avg* term (4), (7) and *var* term (5), (8) come from *average value* and *variance value* in statistics, indicating the average performance and the fluctuation around the mean value across multiple environments respectively. Considering the practical case of depth prediction, it should be more rigorous to prevent the fluctuation of better results than that of worse results under changing conditions. We then propose the *relative deviation* term (6), (9) to calculate the relative difference between maximum and minimum of all the environments. So we formulate *relative deviation* terms for *AbsRel* and $1 - a_1$, which are the less the better and more strict than the *variance* terms (5), (8).

B. Evaluated Algorithms

As introduced in II-B, the best open-source depth prediction methods on *KITTI* benchmark [13] we have evaluated on the *SeasonDepth* dataset include supervised, semi-supervised and self-supervised methods. For the supervised methods, we choose *VNL* [14], *MegaDepth* [15] and *SGRL* [16]. *VNL* proposes the virtual normal which utilizes a stable geometric constraint for long-range relations in a global view and helps depth prediction. *MegaDepth* introduces an end-to-end hourglass network for depth prediction with several scale-invariant and ordinal depth loss using semantic and geometric information and validation on multiple datasets. *SGRL* uses a novel sampling strategy for better structure and important regions from sparse depth map through Structure-Guided Ranking Loss and conducts cross-dataset validation. Also, semi-supervised method *semiDepth* [17] is also benchmarked, which explicitly exploits left-right consistency as a loss function along with supervised learning.

We choose *adareg* [18], *monoResMatch* [19], *Monodepth2* [20] and *PackNet* [21] as unsupervised or self-supervised methods for depth prediction. *adareg* introduces a novel bilateral consistency constraint on the left-right disparity and adaptive regularization technique. *monoResMatch* leverages traditional stereo algorithms to find proxy labels to predict depth maps in a self-supervised way. *Monodepth2* proposes a simple model using geometric information for robustness

under occlusions and camera motion cases. *PackNet* uses a self-supervised method combining geometry with novel symmetrical packing and unpacking blocks using 3D convolutions for depth prediction.

While for models trained on the *V-KITTI* dataset with multiple environments, we use the two recent competitive algorithms *T2Net* [22] and *GASDA* [23] as baselines. *T2Net* is fully supervised both on *KITTI* and virtual *KITTI* dataset and it enables the training of both synthetic-to-real translation and depth prediction simultaneously. While *GASDA* is unsupervised for real-world images by incorporating geometry-aware loss through wrapping of stereo images together with image translation from synthetic to real-world domain. The evaluation results are shown in section V.

V. ZERO-SHOT EXPERIMENTAL EVALUATION

In this section, supervised and semi-supervised methods *VNL* [14], *MegaDepth* [15] *SGRL* [16] and *semiDepth* [17], unsupervised and self-supervised methods *adareg* [18], *monoResMatch* [19], *Monodepth2* [20] and *PackNet* [21] and methods trained on multi-environment virtual datasets *T2Net* [22] and *GASDA* [23] are evaluated with the metrics introduced in Section IV-A on the test set of *SeasonDepth* with 4 slices about 18367 images, directly using state-of-the-art well-pretrained models from *KITTI* benchmark. Specifically, for *adareg*, *GASDA*, *MegaDepth* and *SGRL*, we use the single released model for evaluation. Besides, we use *mono+stereo,640x192* for *Monodepth2*, *KITTI* pre-trained model for *monoResMatch*, *ResNet18*, *self-supervised*, *192x640* with *ImageNet* for *PackNet*, *Resnet50*, *Eigen finetuned*, *CityScape* for *semiDepth*, *weakly-supervised*, *outdoor* for *T2Net* and *KITTI* pretrained model for *VNL*.

A. Evaluation Comparison from Overall Metrics

From the benchmark of current open-source best depth prediction baselines in Table II, it could be seen that all the methods perform worse on the challenging *SeasonDepth* dataset than *KITTI* dataset. *VNL* [14], *semiDepth* [17] and *Monodepth2* [20] present relatively impressive results on both *KITTI* and *SeasonDepth* dataset. While *MegaDepth* [15] performs better than other baselines on *SeasonDepth* compared to *KITTI*, showing the significance of scale-invariant and ordinal depth loss for training on scaleless dataset and validation on multiple datasets. Additionally, *PackNet* [21] and *monoResMatch* [19] show limited generalization ability compared with other methods on *SeasonDepth* although they perform relatively well on *KITTI*.

For *AbsRel* of *SeasonDepth* Average and Variance, geometric-constraint-free methods *SGRL* [16] and *T2Net* [22] perform relatively worse than other methods, from which it could be inferred that geometry information is essential to the robustness of monocular depth prediction under changing environments. Focused on *SeasonDepth* Average, *SGRL* [16] and *PackNet* [21] perform better on a_1 compared to *AbsRel*, which gives the hint that their bad performance on *AbsRel* might be owing to the extreme but limited outliers of depth map across multiple environments.

TABLE II
EVALUATION RESULTS ON *KITTI* AND *SeasonDepth* DATASET

Method	<i>KITTI</i>		<i>SeasonDepth</i> Average		<i>SeasonDepth</i> Variance		<i>SeasonDepth</i> Deviation	
	<i>AbsRel</i> lower better	a_1 higher better	<i>AbsRel</i> lower better	a_1 higher better	<i>AbsRel</i> (10^{-2}) lower better	a_1 (10^{-2}) lower better	<i>AbsRel</i> lower better	a_1 lower better
VNL [14]	0.0720	0.938	0.297	0.543	0.114	0.187	0.476	0.397
MegaDepth [15]	0.220	0.632	0.505	0.426	0.0883	0.0338	0.197	0.128
SGRL [16]	0.179	0.746	1.15	0.417	0.577	0.0305	0.229	0.0974
semiDepth [17]	0.0784	0.923	0.406	0.465	0.119	0.104	0.276	0.190
adareg [18]	0.126	0.840	0.510	0.416	0.116	0.0579	0.224	0.132
Monodepth2 [20]	0.106	0.876	0.403	0.451	0.0568	0.0695	0.225	0.170
monoResMatch [19]	0.096	0.890	0.483	0.391	0.306	0.103	0.440	0.181
PackNet [21]	0.116	0.865	0.718	0.429	0.173	0.0612	0.196	0.146
T2Net [22]	0.168	0.769	0.807	0.400	0.405	0.0747	0.256	0.148
GASDA [23]	0.143	0.836	0.434	0.409	0.111	0.0654	0.305	0.184

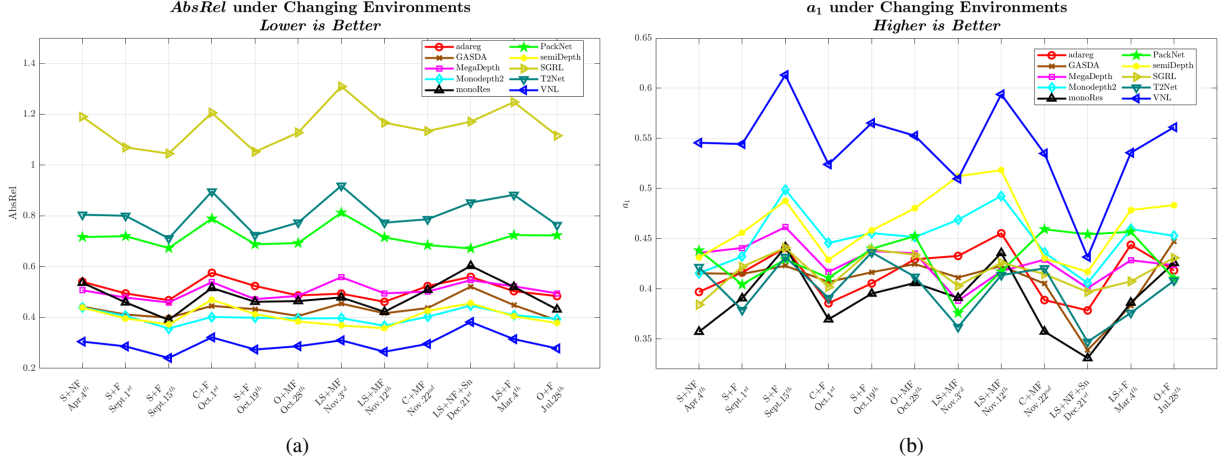


Fig. 5. Diagram (a) (b) are the detailed evaluation results for *AbsRel* and a_1 on *SeasonDepth* dataset under 12 different environments with dates. The abbreviations of X-tick labels are *S* for *Sunny*, *C* for *Cloudy*, *O* for *Overcast*, *LS* for *Low Sun*, *Sn* for *Snow*, *F* for *Foliage*, *NF* for *No Foliage*, and *MF* for *Mixed Foliage*.

Coming to the *Variance* and *Deviation*, thanks to the effective cross-dataset validation *MegaDepth* [15] gives relatively stable performance on both *AbsRel* and a_1 across multiple environments and *SGRL* [16] shows impressive performance on *Variance* and *Deviation* of a_1 metric though bad performance on *AbsRel* Average and *Variance*. On the contrary, although *VNL* [14] and *semiDepth* [17] perform the best on *KITTI* and *SeasonDepth* Average, they clearly suffer from large fluctuation under changing environments from *Variance* and *Deviation*, especially on a_1 metric.

B. Performance under Different Environmental Conditions

The evaluated performance under different environments is illustrated in Figure 5 using lines in different colors and markers. From Figure 5-(a), it could be found that although different methods perform differently on *AbsRel*, the influence of some environments is similar for all the methods. Most methods perform well under *Sunny+Foliage* on *Sept. 15th*, which is close to the environmental condition of *KITTI* dataset. However, *Cloudy+Foliage* on *Oct. 1st*, *Low Sun+Mixed Foliage* on *Nov. 3rd* and *Low Sun+No Foliage+Snow* on *Dec. 21st* pose great challenge to depth prediction for most algorithms.

While from Figure 5-(b), the trend of a_1 from environmental impact is less consistent among all the algorithms but mainly similar to that on *AbsRel*, especially for good performance for *Sunny+Foliage* on *Sept. 15th* and bad per-

formance for *Low Sun+No Foliage+Snow* on *Dec. 21st*. For example, except *MegaDepth* [15], *PackNet* [21] and *SGRL* [16], *Low Sun+No Foliage+Snow* on *Dec. 21st* largely affects the performance of depth prediction, indicating there is still a long way to go for the robust long-term depth prediction. However, multi-environment virtual synthetic dataset with domain adaptation is beneficial to the robustness to changing environments from the performance of *T2Net* [22] and *GASDA* [23] though the only bad results on the snowy weather which is not included in the synthetic *V-KITTI* dataset.

VI. CONCLUSION

In this paper, a new dataset *SeasonDepth* and evaluation metrics are developed for the monocular depth prediction under different environments. Supervised, semi-supervised and self-supervised best open-source depth prediction algorithms from *KITTI* benchmark are evaluated. Through the experimental evaluation, we find that there is still a long way to go to achieve robust long-term monocular depth prediction. Several promising aspects for the future work lie in geometry information involved in the model training and scale-invariant loss to improve the generalization ability. Besides, multi-dataset validation and domain adaptation with training on virtual dataset with images under multiple environmental conditions are beneficial to the robustness under changing real-world environments.

REFERENCES

- [1] D. Eigen, C. Puhrsch, and R. Fergus, "Depth map prediction from a single image using a multi-scale deep network," in *Advances in neural information processing systems*, 2014, pp. 2366–2374.
- [2] F. Liu, C. Shen, G. Lin, and I. Reid, "Learning depth from single monocular images using deep convolutional neural fields," *IEEE transactions on pattern analysis and machine intelligence*, vol. 38, no. 10, pp. 2024–2039, 2015.
- [3] I. Laina, C. Rupprecht, V. Belagiannis, F. Tombari, and N. Navab, "Deeper depth prediction with fully convolutional residual networks," in *2016 Fourth international conference on 3D vision (3DV)*. IEEE, 2016, pp. 239–248.
- [4] D. Xu, E. Ricci, V. Ouyang, X. Wang, and N. Sebe, "Multi-scale continuous crfs as sequential deep networks for monocular depth estimation," in *Proceedings of the IEEE Conference on Computer Vision and Pattern Recognition*, 2017, pp. 5354–5362.
- [5] T. Sattler, W. Maddern, C. Toft, A. Torii, L. Hammarstrand, E. Stenborg, D. Safari, M. Okutomi, M. Pollefeys, J. Sivic, *et al.*, "Benchmarking 6dof outdoor visual localization in changing conditions," in *Proceedings of the IEEE Conference on Computer Vision and Pattern Recognition*, 2018, pp. 8601–8610.
- [6] R. Ranftl, K. Lasinger, D. Hafner, K. Schindler, and V. Koltun, "Towards robust monocular depth estimation: Mixing datasets for zero-shot cross-dataset transfer," *IEEE Transactions on Pattern Analysis and Machine Intelligence*, 2020.
- [7] J. Spencer, R. Bowden, and S. Hadfield, "Defeat-net: General monocular depth via simultaneous unsupervised representation learning," in *Proceedings of the IEEE/CVF Conference on Computer Vision and Pattern Recognition (CVPR)*, June 2020.
- [8] M. Larsson, E. Stenborg, L. Hammarstrand, M. Pollefeys, T. Sattler, and F. Kahl, "A cross-season correspondence dataset for robust semantic segmentation," in *Proceedings of the IEEE Conference on Computer Vision and Pattern Recognition*, 2019, pp. 9532–9542.
- [9] M. Larsson, E. Stenborg, C. Toft, L. Hammarstrand, T. Sattler, and F. Kahl, "Fine-grained segmentation networks: Self-supervised segmentation for improved long-term visual localization," in *Proceedings of the IEEE International Conference on Computer Vision*, 2019, pp. 31–41.
- [10] T. Jenicik and O. Chum, "No fear of the dark: Image retrieval under varying illumination conditions," in *Proceedings of the IEEE International Conference on Computer Vision*, 2019, pp. 9696–9704.
- [11] H. Badino, D. Huber, and T. Kanade, "The CMU Visual Localization Data Set," <http://3dvis.ri.cmu.edu/data-sets/localization>, 2011.
- [12] A. Geiger, P. Lenz, and R. Urtasun, "Are we ready for autonomous driving? the kitti vision benchmark suite," in *2012 IEEE Conference on Computer Vision and Pattern Recognition*. IEEE, 2012, pp. 3354–3361.
- [13] J. Uhrig, N. Schneider, L. Schneider, U. Franke, T. Brox, and A. Geiger, "Sparsity invariant cnns," in *International Conference on 3D Vision (3DV)*, 2017.
- [14] W. Yin, Y. Liu, C. Shen, and Y. Yan, "Enforcing geometric constraints of virtual normal for depth prediction," in *Proceedings of the IEEE International Conference on Computer Vision*, 2019, pp. 5684–5693.
- [15] Z. Li and N. Snavely, "Megadepth: Learning single-view depth prediction from internet photos," in *Proceedings of the IEEE Conference on Computer Vision and Pattern Recognition*, 2018, pp. 2041–2050.
- [16] K. Xian, J. Zhang, O. Wang, L. Mai, Z. Lin, and Z. Cao, "Structure-guided ranking loss for single image depth prediction," in *Proceedings of the IEEE/CVF Conference on Computer Vision and Pattern Recognition*, 2020, pp. 611–620.
- [17] A. J. Amiri, S. Y. Loo, and H. Zhang, "Semi-supervised monocular depth estimation with left-right consistency using deep neural network," in *2019 IEEE International Conference on Robotics and Biomimetics (ROBIO)*. IEEE, 2019, pp. 602–607.
- [18] A. Wong and S. Soatto, "Bilateral cyclic constraint and adaptive regularization for unsupervised monocular depth prediction," in *Proceedings of the IEEE Conference on Computer Vision and Pattern Recognition*, 2019, pp. 5644–5653.
- [19] F. Tosi, F. Aleotti, M. Poggi, and S. Mattoccia, "Learning monocular depth estimation infusing traditional stereo knowledge," in *Proceedings of the IEEE Conference on Computer Vision and Pattern Recognition*, 2019, pp. 9799–9809.
- [20] C. Godard, O. M. Aodha, M. Firman, and G. J. Brostow, "Digging into self-supervised monocular depth estimation," in *Proceedings of the IEEE International Conference on Computer Vision*, 2019, pp. 3828–3838.
- [21] V. Guizilini, R. Ambrus, S. Pillai, A. Raventos, and A. Gaidon, "3d packing for self-supervised monocular depth estimation," in *Proceedings of the IEEE/CVF Conference on Computer Vision and Pattern Recognition*, 2020, pp. 2485–2494.
- [22] C. Zheng, T.-J. Cham, and J. Cai, "T2net: Synthetic-to-realistic translation for solving single-image depth estimation tasks," in *Proceedings of the European Conference on Computer Vision (ECCV)*, 2018, pp. 767–783.
- [23] S. Zhao, H. Fu, M. Gong, and D. Tao, "Geometry-aware symmetric domain adaptation for monocular depth estimation," in *Proceedings of the IEEE Conference on Computer Vision and Pattern Recognition*, 2019, pp. 9788–9798.
- [24] A. Gaidon, Q. Wang, Y. Cabon, and E. Vig, "Virtual worlds as proxy for multi-object tracking analysis," in *Proceedings of the IEEE conference on computer vision and pattern recognition*, 2016, pp. 4340–4349.
- [25] N. Silberman, D. Hoiem, P. Kohli, and R. Fergus, "Indoor segmentation and support inference from rgb-d images," in *European conference on computer vision*. Springer, 2012, pp. 746–760.
- [26] Y. Kim, H. Jung, D. Min, and K. Sohn, "Deep monocular depth estimation via integration of global and local predictions," *IEEE transactions on Image Processing*, vol. 27, no. 8, pp. 4131–4144, 2018.
- [27] T. Koch, L. Liebel, F. Fraundorfer, and M. Körner, "Evaluation of cnn-based single-image depth estimation methods," in *European Conference on Computer Vision Workshop (ECCV-Ws)*, L. Leal-Taixé and S. Roth, Eds. Springer International Publishing, 2018, pp. 331–348.
- [28] C. Wang, S. Lucey, F. Perazzi, and O. Wang, "Web stereo video supervision for depth prediction from dynamic scenes," in *2019 International Conference on 3D Vision (3DV)*. IEEE, 2019, pp. 348–357.
- [29] K. Xian, C. Shen, Z. Cao, H. Lu, Y. Xiao, R. Li, and Z. Luo, "Monocular relative depth perception with web stereo data supervision," in *The IEEE Conference on Computer Vision and Pattern Recognition (CVPR)*, June 2018.
- [30] A. Saxena, M. Sun, and A. Y. Ng, "Make3d: Learning 3d scene structure from a single still image," *IEEE transactions on pattern analysis and machine intelligence*, vol. 31, no. 5, pp. 824–840, 2008.
- [31] M. Cordts, M. Omran, S. Ramos, T. Rehfeld, M. Enzweiler, R. Benenson, U. Franke, S. Roth, and B. Schiele, "The cityscapes dataset for semantic urban scene understanding," in *Proceedings of the IEEE conference on computer vision and pattern recognition*, 2016, pp. 3213–3223.
- [32] W. Chen, Z. Fu, D. Yang, and J. Deng, "Single-image depth perception in the wild," in *Advances in neural information processing systems*, 2016, pp. 730–738.
- [33] G. Ros, L. Sellart, J. Materzynska, D. Vazquez, and A. M. Lopez, "The synthia dataset: A large collection of synthetic images for semantic segmentation of urban scenes," in *Proceedings of the IEEE conference on computer vision and pattern recognition*, 2016, pp. 3234–3243.
- [34] A. Saxena, S. H. Chung, and A. Y. Ng, "Learning depth from single monocular images," in *Advances in neural information processing systems*, 2006, pp. 1161–1168.
- [35] B. Liu, S. Gould, and D. Koller, "Single image depth estimation from predicted semantic labels," in *2010 IEEE Computer Society Conference on Computer Vision and Pattern Recognition*. IEEE, 2010, pp. 1253–1260.
- [36] X. Wang, D. Fouhey, and A. Gupta, "Designing deep networks for surface normal estimation," in *Proceedings of the IEEE Conference on Computer Vision and Pattern Recognition*, 2015, pp. 539–547.
- [37] J. Hu, Y. Zhang, and T. Okatani, "Visualization of convolutional neural networks for monocular depth estimation," in *Proceedings of the IEEE International Conference on Computer Vision*, 2019, pp. 3869–3878.
- [38] H. Fu, M. Gong, C. Wang, K. Batmanghelich, and D. Tao, "Deep ordinal regression network for monocular depth estimation," in *Proceedings of the IEEE Conference on Computer Vision and Pattern Recognition*, 2018, pp. 2002–2011.
- [39] U. Kusupati, S. Cheng, R. Chen, and H. Su, "Normal assisted stereo depth estimation," in *Proceedings of the IEEE/CVF Conference on Computer Vision and Pattern Recognition (CVPR)*, June 2020.
- [40] C. Godard, O. Mac Aodha, and G. J. Brostow, "Unsupervised monocular depth estimation with left-right consistency," in *Proceedings of*

the IEEE Conference on Computer Vision and Pattern Recognition, 2017, pp. 270–279.

- [41] J. Watson, M. Firman, G. J. Brostow, and D. Turmukhambetov, “Self-supervised monocular depth hints,” in *Proceedings of the IEEE International Conference on Computer Vision*, 2019, pp. 2162–2171.
- [42] H. Zhan, R. Garg, C. Saroj Weerasekera, K. Li, H. Agarwal, and I. Reid, “Unsupervised learning of monocular depth estimation and visual odometry with deep feature reconstruction,” in *Proceedings of the IEEE Conference on Computer Vision and Pattern Recognition*, 2018, pp. 340–349.
- [43] R. Garg, V. K. BG, G. Carneiro, and I. Reid, “Unsupervised cnn for single view depth estimation: Geometry to the rescue,” in *European Conference on Computer Vision*. Springer, 2016, pp. 740–756.
- [44] T. Zhou, M. Brown, N. Snavely, and D. G. Lowe, “Unsupervised learning of depth and ego-motion from video,” in *Proceedings of the IEEE Conference on Computer Vision and Pattern Recognition*, 2017, pp. 1851–1858.
- [45] A. Johnston and G. Carneiro, “Self-supervised monocular trained depth estimation using self-attention and discrete disparity volume,” in *Proceedings of the IEEE/CVF Conference on Computer Vision and Pattern Recognition (CVPR)*, June 2020.
- [46] Y. Chen, W. Li, X. Chen, and L. V. Gool, “Learning semantic segmentation from synthetic data: A geometrically guided input-output adaptation approach,” in *Proceedings of the IEEE Conference on Computer Vision and Pattern Recognition*, 2019, pp. 1841–1850.
- [47] B. Bozorgtabar, M. S. Rad, D. Mahapatra, and J.-P. Thiran, “Syndemo: Synergistic deep feature alignment for joint learning of depth and ego-motion,” in *Proceedings of the IEEE International Conference on Computer Vision*, 2019, pp. 4210–4219.
- [48] J. L. Schönberger, E. Zheng, J.-M. Frahm, and M. Pollefeys, “Pixel-wise view selection for unstructured multi-view stereo,” in *European Conference on Computer Vision*. Springer, 2016, pp. 501–518.
- [49] J. L. Schönberger and J.-M. Frahm, “Structure-from-motion revisited,” in *Proceedings of the IEEE Conference on Computer Vision and Pattern Recognition*, 2016, pp. 4104–4113.